6-1-2018

Solution and Solid-State Characterization of Zn(II) Complexes Containing A New Tridentate N_2s Ligand

Valerie Tran
Boise State University

Kate E. Allen
Boise State University

Martin Garcia Chavez
Boise State University

Christopher Aaron
Boise State University

Joseph J. Dumais
Boise State University

See next page for additional authors

Publication Information

Tran, Valerie; Allen, Kate E.; Garcia Chavez, Martin; Aaron, Christopher; Dumais, Joseph J.; York, John T.; and Brown, Eric C. (2018). "Solution and Solid-State Characterization of Zn(II) Complexes Containing A New Tridentate N2s Ligand". *Polyhedron, 147,* 131-141.
http://dx.doi.org/10.1016/j.poly.2018.03.008

Authors
Valerie Tran, Kate E. Allen, Martin Garcia Chavez, Christopher Aaron, Joseph J. Dumais, John T. York, and Eric C. Brown

Solution and Solid-State Characterization of Zn(II) Complexes Containing a New Tridentate N_2S Ligand

Valerie Tran[†], Kate E. Allen[†], Martin Garcia Chavez[†], Christopher Aaron[†], Joseph J. Dumais[†], John T. York[‡], and Eric C. Brown[†]*

†Department of Chemistry, Boise State University, Boise, ID 83725

‡Department of Chemistry, Stetson University, DeLand, FL 32723

Tel: 208-426-1186

Fax: 208-426-1311

E-mail: *ericbrown3@boisestate.edu*

*To whom all correspondence should be addressed

Abstract

A new N_2S ligand bis(pyridyl)(2-mercapto-1-methylimidazolyl)methane (**2**, Py_2MeImS) has been synthesized and characterized. Treatment of this ligand with bromide and triflate salts of Zn(II) results in the complexes $(Py_2MeImS)ZnBr_2$ (**3**) and $[(Py_2MeImS)_2Zn](OTf)_2$ (**4**), respectively. The solid-state structure of $(Py_2MeImS)ZnBr_2$ shows bidentate N,N-coordination of Py_2MeImS to the zinc ion, with the sulfur atom of the 2-mercaptoimidazole moiety uncoordinated. Two conformers of **3** rapidly interconvert in solution at room temperature, and variable temperature NMR studies and DFT calculations were used to help assign the likely identity of these conformers. In contrast, the crystal structure of $[(Py_2MeImS)_2Zn](OTf)_2$ exhibits a zinc ion with a distorted octahedral geometry where the two sulfur atoms of the two ligands are coordinated to the zinc center in a *cis*-configuration. Even though the *cis*-isomer (**4-cis**) is calculated to be lower in energy than the *trans*-isomer (**4-trans**), the low temperature ^1H NMR spectrum of **4** reveals a single symmetric species that is inconsistent with the *cis*-isomer observed in the solid-state structure. DFT calculations propose alternative higher energy structures, including a *trans*-configuration of the coordinated S-atoms of the two Py_2MeImS ligands, as well as structures in which the 2-mercaptoimidazole groups are no longer coordinated to the zinc(II) center. These studies provide valuable insight into the potential binding modes of this new ligand and its behavior in solution.

Keywords

NMR spectroscopy; density functional theory calculations; single crystal X-ray crystal structures; zinc(II) complexes; fluxionality.

1. Introduction

The coordination chemistry of zinc ions complexed with ligands capable of binding through a sulfur and two nitrogen donors has attracted attention because of its relevance to modeling zinc-containing enzymes with [N_2S] structural binding motifs. For instance, bacteriophage T7 lysozyme [1], peptide deformylase (in plants PDF1A) [2], and bovine 5-aminolevulinate dehydratase [3] all contain active sites consisting of a pseudo-tetrahedral zinc ion bound to a cysteine and two histidine residues with the fourth binding site occupied by a water molecule. The combined nitrogen and sulfur ligation is an important component for tuning the zinc center and activating the water nucleophile. As such, the development of new [N_2S] ancillary ligands to support the synthesis and study of model complexes is crucial to the further understanding of these biological compounds.

Synthetic efforts to prepare zinc complexes with a [N_2S] facial binding motif have primarily used heteroscorpionate-based ligands containing alkyl or aryl thiolates. These ligands have been successfully used to make tetrahedral [N_2S]ZnX complexes, where X = halide, –CH_3, –hydroxamate or –SR′ [4]. Alternatively, new heteroscorpionate ligands where mercaptoimidazolyl groups have replaced alkyl and aryl thiolates as the sulfur atom donor(s) have been successfully used to model sulfur-rich active sites [5]. The sulfur atom of the mercaptoimidazolyl moiety is expected to have a significant negative charge similar to thiourea (charge = −0.37 e) [6] and, as such, have been coined by Vahrenkamp [7] as a “tame” thiolate donor. An example of an [N_2S] ligand containing a mercaptoimidazolyl group is the ligand bis(pyrazolyl)(2-mercapto-1-methylimidazolyl)hydroborato ligand ($BpMt^{Me}$, Chart 1) [8].

For the purpose of comparison, we chose to prepare and examine the coordination chemistry of a new tridentate ligand bis(pyridyl)(2-mercapto-1-methylimidazolyl)methane (Py_2MeImS, Chart 1) that is closely related to $BpMt^{Me}$. Py_2MeImS does not contain a central boron atom, which should allow us to explore the influence of the charge of the ligands on the structures and electronic properties of the complexes. Here, we describe the coordination chemistry of the Py_2MeImS ligand with zinc salts containing coordinating and weakly-coordinating anions. These new complexes provide important insight into both the solid-state and solution-phase behavior of the ligand and its potential binding modes. Computational studies provide further insight into the properties of the Py_2MeImS ligand and how they compare to existing ligand systems.

2. Experimental Section

2.1. General

All reactions were performed using standard Schlenk techniques under an atmosphere of dry nitrogen gas. Solvents and reagents were obtained from commercial sources in analytical grade quality and used as received unless noted otherwise. The solvents tetrahydrofuran (THF), methanol (MeOH), and dioxane were dried with CaH_2 and distilled prior to use. NMR spectra were recorded on a Bruker AVANCE III 600 MHz NMR or Bruker AVANCE III 300 MHz NMR. Chemical shifts were expressed in parts per million (ppm) and referenced to residual solvent as the internal reference for ^{1}H ($CDCl_3$: δ = 7.26 ppm or CD_3OD: δ = 3.31 ppm) and ^{13}C ($CDCl_3$: δ = 77.16 ppm and CD_3OD: δ = 49.00 ppm). The NMR probe temperatures were calibrated using the chemical shift separation between the CH_3 and the –OH peaks of a solution of 4% CH_3OH in CD_3OD. IR spectra were measured using a Perkin Elmer Spectrum 100 spectrometer. Elemental analyses were performed by Atlantic Microlabs of Norcross, GA. High resolution mass spectrometry (HRMS) of Py_2MeImS (**2**) was obtained using an ultrahigh resolution Maxis QTOF

(Bruker Daltonics) instrument. The compound bis(2-pyridyl)bromomethane was made by a previously reported procedure [9].

2.2. Synthesis and characterization

*2.2.1. Preparation of [Py_2MeImH]Br (**1**)*

To a solution of bis(2-pyridyl)bromomethane (2.21 g, 8.86 mmol) dissolved in dioxane (50 mL) was added 1-methylimidazole (0.73 g, 8.86 mmol). The solution was refluxed overnight, which resulted in a tan brown precipitate. The precipitate was collected, washed with ether (2 x 10 mL) and then dried under reduced pressure (1.55 g, 53%). ^{1}H NMR ($CDCl_3$, 300 MHz): δ 10.40 (br dd, 1H), 8.55 (d, J = 4.9 Hz, 2H), 8.20 (s, 1H), 8.19 (dd, J = 1.7, 1.7 Hz, 1H), 7.80-7.68 (m, 4H), 7.35 (dd, J = 1.7, 1.7 Hz, 1H), 7.30-7.22 (m, 2H), 4.05 (s, 3H). ^{13}C{^{1}H} NMR ($CDCl_3$, 150 MHz) δ 154.7, 149.7, 137.6, 137.4, 124.3, 123.9, 123.7, 122.0, 66.3, 36.9. IR (ATR, cm^{-1}): 3091 (m), 3041 (m), 2994 (m), 1680 (w), 1588 (m), 1571 (m), 1548 (m), 1474 (m), 1446 (w), 1428 (s), 1321 (m), 1210 (w), 1162 (s), 1082 (m), 1052 (m), 994 (m), 950 (w), 883 (w), 848 (m), 770(s), 752 (s), 738 (s), 689 (m), 670 (s).

*2.2.2 Preparation of Py_2MeImS (**2**)*

To a solution of [Py_2MeImH]Br (**1**) (1.48 g, 4.49 mmol) dissolved in methanol (50 mL) was added elemental sulfur (0.36 g, 11.22 mmol) and potassium *tert*-butoxide (0.50 g, 4.49 mmol). The solution was refluxed overnight before being cooled to room temperature and water (20 mL) added. The solution was then extracted with dichloromethane (5 x 20 mL), dried with anhydrous $MgSO_4$, filtered and the solvent removed under reduced pressure. Crude Py_2MeImS (**2**) was purified by column chromatography (silica gel; DCM followed by EtOAc) to afford Py_2MeImS

(**2**) as a yellow oil (0.27 g, 21%). ^{1}H NMR ($CDCl_3$, 600 MHz): δ 8.59 (d, J = 4.8 Hz, 2H), 7.72 (td, J = 7.7, 7.7, 1.6 Hz, 2H), 7.64 (s, 1H), 7.37 (d, J = 7.7 Hz, 2H), 7.27 (d, J = 2.5 Hz, 1H), 7.24 (dd, J = 7.4, 5.0 Hz, 2H), 6.67 (d, J = 2.5 Hz, 1H), 3.64 (s, 3H). $^{13}C\{^{1}H\}$ NMR ($CDCl_3$, 150 MHz): δ 163.5, 157.0, 149.5, 137.5, 124.2, 123.2, 117.6, 117.2, 65.5, 35.4. IR (ATR, cm^{-1}): 3053 (w), 3005 (w), 1682 (s), 1582 (m), 1568 (m), 146 6(w), 1430 (m), 1315 (s), 1280 (m), 1241 (m), 1227 (m), 1182 (w), 1150 (w), 1090 (w), 1047 (w), 993 (s), 944 (s), 827 (m), 784 (m), 743 (s), 694 (m), 661 (s). HRMS (ESI, Pos) calculated for $[C_{15}H_{14}N_4S_1 + Na]^+$: 305.0831, found 305.0844.

*2.2.3 Preparation of (Py_2MeImS)$ZnBr_2$ (**3**)*

To a solution of Py_2MeImS (**2**) (0.13 g, 0.46 mmol) dissolved in methanol (25 mL) was added anhydrous $ZnBr_2$ (0.105 g, 0.46 mmol). The solution was heated to reflux, resulting in a white precipitate, and stirred overnight. The white solid was collected by filtration, washed with diethyl ether (3 x 5 mL) and dried under reduced pressure to afford (Py_2MeImS)$ZnBr_2$ (**3**) (0.174 g, 74%). Colorless crystals suitable for crystallographic characterization were obtained by diethyl ether diffusion into dichloromethane at room temperature. ^{1}H NMR (600 MHz, $CDCl_3$, −48 °C), conformer **3a**: δ 8.81 (2H), 8.38 (1H), 8.04 (1H), 7.91 (4H), 7.52 (2H), 6.91 (1H), 3.73 (3H); conformer **3b**: δ 8.92 (2H), 8.23 (1H), 8.11 (4H), 7.83 (1H), 7.75 (2H), 6.68 (1H), 3.62 (3H). IR (ATR, cm^{-1}): 3528 (w), 3173 (w), 3133 (w), 3104 (w), 2810 (w), 1602 (s), 1575 (m), 1467 (s), 1455 (s), 1436 (s), 1390 (s), 1359 (m), 1337 (w), 1298 (w), 1232 (s), 1162 (w), 1136 (m), 1100 (m), 1062 (m), 1026 (s), 914 (w), 868 (m), 828 (s), 767v(m), 766 (s), 716 (s), 681 (s). Analysis Calculated for $C_{15}H_{14}Br_2N_4SZn$: C, 35.49; H, 2.78; N, 11.04%. Found: C, 35.34; H, 2.95; N, 10.50%.

*2.2.4 Preparation of [(Py$_2$MeImS)$_2$Zn](OTf)$_2$ (**4**)*

To a solution of Py$_2$MeImS (**2**) (0.10 g, 0.35 mmol) dissolved in methanol (14 mL) was added Zn(OTf)$_2$ (0.064 g, 0.18 mmol). The solution was stirred for 18 hr before the volume was reduced to 5 mL under reduced pressure. The addition of diethyl ether (15 mL) resulted in the formation of a white solid, which was collected, washed with diethyl ether (3 x 10 mL) and dried under reduced pressure to afford [(Py$_2$MeImS)$_2$Zn](OTf)$_2$ (**3**) (0.089 g, 54%). Colorless crystals suitable for crystallographic characterization were obtained by diethyl ether diffusion into dichloromethane at room temperature. ^{1}H NMR (CD$_3$OD, 10 mM, -35 ºC): δ 8.55 (d, J = 4.4 Hz, 2H), 7.90 (t, J = 7.7 Hz, 2H), 7.48 (s, 1H), 7.44 (dd, J = 7.0, 5.2 Hz, 2H), 7.29 (dd, J = 7.7, 4.8 Hz, 2H), 7.12 (d, J = 2.2 Hz, 1H), 7.09-7.06 (m, 1H), 3.61 (s, 3H). ^{13}C{^{1}H} NMR (CD$_3$OD, 10 mM, -35 ºC): δ163.7, 158.2, 150.5, 139.3, 125.2, 124.8, 120.0, 117.4, 67.0, 35.4. IR (ATR, cm^{-1}): 3170 (w), 3115 (w), 1602 (m), 1578 (w), 1487 (w), 1466 (w), 1436 (m), 1400 (w), 1367 (w), 1252 (s), 1224 (s), 1153 (s), 1100 (w), 1065 (w), 1029 (s), 910 (w), 898 (w), 833 (w), 762 (m), 678 (m). Anal. calcd for $C_{32}H_{28}ZnN_8O_6S_4F_6$: C, 41.40; H, 3.04; N, 12.07%. Found: C, 41.14; H, 3.03; N, 11.83%.

2.3. X-ray Crystallography

Crystals suitable for X-ray diffraction were obtained from slow vapor diffusion and mounted on a glass fiber using hydrocarbon oil and cooled under a nitrogen stream to 150(1) K. A Nonius Kappa CCD diffractometer (Mo Kα radiation; λ = 0.71073 Å) was used for data collection. Unit cell parameters were determined from 10 data frames with an oscillation range of 1 deg/frame and an exposure time of 20 sec/frame. Indexing and unit cell refinement based on the reflections from the initial set of frames were consistent with monoclinic *P* lattices for **3** and **4**. The intensity

data for each compound was then collected. These reflections were then indexed, integrated and corrected for Lorentz, polarization and absorption effects using DENZO-SMN and SCALEPAC [10]. The space group for each compound was determined from the systematic absences in the diffraction data. The structures were solved by a combination of direct and heavy atom methods using SIR 97 [11]. All non-hydrogen atoms were refined with anisotropic displacement parameters. All hydrogen atoms were placed in ideal positions and assigned isotropic displacement coefficients U(H) = 1.2U(C) or 1.5U(C_{methyl}) and allowed to ride on their respective carbons using SHELXL-97 [12]. A summary of the crystallographic data and parameters for **3** and **4** are found in Table 1.

2.4. Computational Methods

Calculations were completed with Gaussian 09W [13] using the ωB97X-D functional [14] unless otherwise noted. This range-separated hybrid meta-GGA functional with empirical dispersion correction has been shown to have excellent success in reproducing geometries and other properties for metal complexes [15]. Optimized geometries were obtained using the Stuttgart-Dresden (SDD) basis set and effective core potential [16] for zinc and the 6-31+g(d,p) basis set [17] for all other atoms (genecp keyword). For all isomers of complex **3**, solvent effects were modeled in the geometry optimizations and all single-point calculations with the CPCM solvation model [18] and chloroform as the solvent, while methanol solvation was used for all conformers of complex **4**. Optimized structures were confirmed as minima by the absence of imaginary frequencies in subsequent analytical frequency calculations unless otherwise noted. All optimizations were completed using tight convergence criteria and the ultrafine grid (opt=tight, int=grid=ultrafine keywords). Solvated single-point energy calculations were completed for

optimized structures using the SDD basis set and effective core potential for zinc and the 6-311+g(2d,p) basis set [19] for all other atoms. Natural population and bond orbital (NBO) calculations [20] were performed on selected complexes using this same basis set combination. Solvated free energies for selected structures were obtained by using the thermodynamic correction factors from the frequency calculations at 298.15 K and 1 atm with the higher level single-point electronic energies. NMR spectra were calculated with the hybrid B3LYP functional [21] using the GIAO method [22] with the 6-311+g(2d,p) basis set for all atoms. This method has been shown to provide good agreement between experimental and calculated NMR parameters [23]. Calculated NMR chemical shifts are reported relative to TMS and were scaled according to the method of Pierens [24] using the appropriate solvent. $CF_3SO_3^-$ anions in the experimental systems were not modeled in these calculations.

3. Results and Discussion

3.1. Synthesis and Characterization of Py_2MeImS Ligand

The ligand Py_2MeImS (**2**) was prepared by a two-step procedure (Scheme 1). Formation of the imidazolium salt [Py_2MeImH]Br (**1**) in a 53% yield was achieved by heating a dioxane solution of Py_2CHBr and 1-methylimidazole. A diagnostic property for formation of the imidazolium cation of **1** is a peak at 10.4 ppm in the ^{1}H NMR spectrum for the acidic proton at the C2 position of the imidazolium ring. Deprotonation of **1** with KO^{t}Bu in the presence of S_8 in methanol resulted in formation of **2**, which was purified by column chromatography. Ligand **2** was fully characterized by ^{1}H and ^{13}C NMR and IR spectroscopy and mass spectrometry (HRMS).

In addition to potential bidentate pyridyl N-donor atoms, this ligand possesses a 2-mercaptoimidazole moiety that can potentially exist in both thione and thiolate tautomers. As

discussed by Parkin [5], the related tris(2-mercapto-1-R–imidazolyl)hydroborato ligands are generally described as possessing primarily thione character. However, natural bond orbital (NBO) calculations predicted that there is significant anionic thiolate character to the S-atom in these ligands (charge = −0.36 e). NBO calculations for both the Py_2MeImS ligand and the analogous bis(pyrazolyl)(2-mercapto-1-methylimidazolyl)hydroborato ligand ($BpMt^{Me}$, Chart 1) were performed to compare the potential electronic properties of these related ligands and the impact of the anionic charge on the boron atom. First, DFT optimizations with chloroform solvation predict that there are two principal rotamers for Py_2MeImS that have slightly different properties (Chart 2): Rotamer a with the 2-mercaptoimidazole group *cis* to the bridging C–*H* proton, and Rotamer b with the 2-mercaptoimidazole group *trans* to the bridging C–*H* proton. Rotamer a is more stable than Rotamer b by ~27 kJ/mol and possesses a slightly longer C–S bond (1.699 versus 1.693Å). This lengthened C–S bond yields a lower calculated Wiberg C–S bond index (1.35 versus 1.38) and a larger calculated negative charge on the S-atom (−0.405 e versus −0.375 e). These properties are indicative of slightly greater thiolate character for Rotamer a and could potentially be related to a weak S···H–C bond interaction with the bridging C–*H* proton (the S···H distance is 2.60 Å). The enhanced stability of Rotamer a might also affect whether the ligand binds in a bidentate or tridentate fashion.

By comparison, the anionic bis(pyrazolyl)(2-mercapto-1-methylimidazolyl)hydroborato ligand is also predicted to have two principal rotamers, with the *cis* rotamer also being more stable than the *trans* rotamer by ~25 kJ/mol. However, unlike the Py_2MeImS ligand, there is no direct S···H–B bond interaction detected in the *cis* rotamer that would account for the increased stability. The NBO-calculated charge for the S-atom of *cis* and *trans* rotamers of the $BpMt^{Me}$ ligand is −0.465 e and −0.446 e, respectively. Therefore, the S-atom of the anionic $BpMt^{Me}$ ligand possesses

15–19% ***more*** negative charge than the neutral Py_2MeImS counterpart, which could lead to significant differences in the behavior of these two ligands. For comparison, it is informative to note that NBO calculations on thioformaldehyde, with a C=S bond length of 1.61Å, predict the S-atom to be nearly neutral (charge = +0.025 e) and to have a C=S Wiberg bond index of 2.04. Given this comparison, both the Py_2MeImS and $BpMt^R$ ligands can be considered to possess significant anionic thiolate character.

3.2. Coordination Chemistry of Py_2MeImS with Zinc Salts Containing Coordinating and Non-Coordinating Anions

To examine the coordination chemistry of the Py_2MeImS ligand, two different Zn^{2+} complexes were prepared by stirring **2** in methanol with the appropriate zinc salt, as shown in Scheme 2. First, the reaction of equimolar amounts of $ZnBr_2$ and Py_2MeImS affords neutral (Py_2MeImS)$ZnBr_2$ (**3**), where the Py_2MeImS ligand acts as a bidentate chelating N-donor ligand and the sulfur atom of the 2-mercapto-1-methylimidazole moiety is not coordinated to the Zn ion. In contrast, the reaction of $Zn(OTf)_2$ with Py_2MeImS, regardless of the stoichiometric ratio, affords the di-cation $[(Py_2MeImS)_2Zn]^{2+}$ (**4**), in which the zinc(II) center is in a distorted octahedral coordination environment and the Py_2MeImS ligand acts as a tridentate chelating ligand with a bound sulfur atom from the mercaptoimidazolyl substituent. Complexes **3** and **4** were characterized by NMR and FT-IR spectroscopy, elemental analysis (CHN) and single-crystal X-ray crystallography.

*3.3. X-ray Structure of (Py_2MeImS)$ZnBr_2$ (**3**)*

The solid-state structure of **3** is shown in Figure 1, with the details of the crystallographic characterization summarized in Table 1. Compound **3** is a monomeric complex with a four-coordinate distorted tetrahedral zinc ion. The zinc center is complexed by two bromides and the Py_2MeImS ligand binds in a bidentate manner through the nitrogen atoms of the two pyridyl rings. Notably absent is any bonding interaction between the 2-mercaptoimidazole sulfur atom and the zinc center. The smallest bond angle is the N1–Zn1–N2 angle (89.56(13)°) and the largest is the Br1–Zn1–Br2 angle (116.96(2)°). The two Zn–Br distances (2.3305(6) and 2.3515(6) Å) are similar to other tetrahedral zinc complexes containing terminal bromides [25]. The average Zn–N distance of 2.043(4) Å compares well with the Zn-N distance of four-coordinated zinc-pyridine compounds [26]. The bidentate coordination of the Py_2MeImS ligand results in the formation of a boat-like metallocycle, with the 2-mercapto-1-methylimidazole group attached to the methine carbon in an equatorial position. The X-ray structure of **3** is also shown overlaid with the DFT-calculated structure in Figure 2, demonstrating good agreement between the calculated structure and the experimental geometry. Of particular note is the C–S bond length of 1.681 Å, which compares very well to the 1.686 Å predicted by DFT calculations. This bond length and the calculated charge of the S-atom in this complex (−0.338 e) indicate significant thiolate character for the sulfur, even though it does not bind to the Zn center.

*3.4. Solution-State NMR Spectroscopy of **3***

Although only a single conformer of compound **3** was characterized in the solid state (**3a**, Figure 3), two additional conformers can arise either from a rotation of the pyridyl rings (**3b**), or from a 180° rotation of the 2-mercaptoimidazole group (**3c**). Indeed, the ^{1}H NMR spectrum of **3** in $CDCl_3$ at 25 °C contains broad signals indicative of a fluxional process. The variable

temperature spectra measured from 25 °C to −48 °C are shown in Figure 4. Lowering the temperature to −48 °C resulted in the formation of two distinct sets of resonances in an approximately 1.5:1 ratio, indicating the presence of two species of relatively similar concentrations. A 2D-EXSY spectrum (Figure 5) at −48 °C allowed the identification of exchanging partners via cross peaks resulting from saturation transfer between the peaks representing protons exchanging positions in the interconverting conformers. Specific proton resonances were subsequently assigned based on the low temperature COSY spectrum (see Figure S1 in supporting information).

To gain some insight into potential isomerization in solution and to aid in identification of the species present, all three conformers were studied using DFT in $CHCl_3$ solvation. The calculated Gibbs free energies of the three species are very similar, with the calculated free energies of **3a** and **3b** being virtually equal ($\Delta G_{a\rightarrow b}$ = −0.4 kJ/mol), while **3c** is slightly higher in energy ($\Delta G_{b\rightarrow c}$ = 5.8 kJ/mol). The calculated $\Delta G_{a\rightarrow b}$ value would yield an equilibrium ratio of **3b** to **3a** of approximately 1.2:1, while the calculated energy of **3c** would lead to its equilibrium concentration in solution being less than 10% of **3b**. Both of these results are consistent with **3a** and **3b** being the minor and major species observed experimentally in the ^{1}H NMR spectrum, respectively.

DFT-calculated ^{1}H NMR spectra of all three conformers were also obtained with $CHCl_3$ solvation for comparison with experimental data (Table 2). As a baseline for comparison, calculated ^{1}H NMR spectra of the free Py_2MeImS ligand indicate that orientation of the 2-mercaptoimidazole ring has a particularly dramatic effect on the chemical shift of the bridging C–*H* proton (labeled H_a in Chart 3). Specifically, in ligand Rotamer a where there is close S···H_a contact (2.60 Å), the chemical shift of H_a is 7.6 ppm. In contrast, in Rotamer b where there is no

S···H_a interaction, the proton resonance is shifted upfield to 6.5 ppm (Figure 6). Thus, close proximity of H_a to the 2-mercaptoimidazole sulfur results in a >1 ppm shift to lower field, similar to the effect observed for hydrogen-bonded protons [27]. Moreover, the calculated value of 7.58 ppm for H_a in the most stable rotamer for free Py_2MeImS (Rotamer a) is in good agreement with the value from the experimental ^{1}H NMR spectrum of the ligand (7.64 ppm). The sensitivity of the chemical shift of H_a to its chemical environment could potentially function as a useful spectroscopic handle for determining the conformation and binding mode of the Py_2MeImS ligand in solution.

With this in mind, the different environment for H_a in conformers **3a**, **3b**, and **3c** would likely lead to differences in its chemical shift, particularly when comparing **3a**/**3b** (where H_a is in contact with the S-atom) and **3c** (where there is no S···H_a interaction). Indeed, H_a is predicted to have very similar chemical shifts in **3a** (8.16 ppm) and **3b** (8.17 ppm), both of which have close S···H_a contact (2.57 Å and 2.52 Å, respectively). These chemical shifts are significantly downfield from that calculated for **3c** (7.57 ppm), consistent with no S···H_a contact in this isomer. COSY and EXSY analysis of **3** in solution reveal chemical shifts for H_a of the interconverting species at 8.04 and 8.23 ppm for the minor and major component, respectively. These values are in the range of those predicted for **3a** and **3b**, consistent with these two species being the interconverting isomers in solution. This is also supported by the low equilibrium concentration predicted for isomer **3c** and the upfield chemical shift of H_a in its calculated ^{1}H NMR spectrum. However, while the predicted shifts for H_a in **3a** and **3b** are in the range of the experimental shifts observed, the similar DFT-calculated values for these two isomers do not allow for a more conclusive determination of the major and minor species in the experimental system.

*3.5. X-ray Structure of [(Py_2MeImS)$_2$Zn](OTf)$_2$ (**4**)*

The solid-state structure of the cationic portion of **4**, along with selected bond distances and angles, is shown in Figure 7, with the most obvious difference from **3** being the direct coordination of the S-atom to the zinc(II) center. A summary of the X-ray crystallographic data and refinement parameters is provided in Table 1. The coordination environment of the zinc ion consists of a six-coordinate slightly distorted octahedron. The two Py_2MeImS ligands facially coordinate the metal ion in a tridentate fashion, with the two sulfur atoms S1 and S2 adopting a *cis*-configuration (S–Zn–S angle of 80.43(2)°). The Zn–$N_{pyridyl}$ distances vary from 2.154(2) to 2.210(2) Å and are unremarkable. However, the Zn–S distances of 2.5078(7) and 2.5353(7) Å are significantly longer than those in other zinc complexes with 2-mercaptoimidazole donors (Zn–S range of 2.30–2.37 Å) [28]. Instead the Zn–S distances in **4** are more typical of Zn–S distances observed in octahedral Zn(II) complexes containing thioethers [29]. Such long Zn–S bonds could also be indicative of weaker interactions, consistent with a lack of coordination for the S-atom of Py_2MeImS observed in **3**.

*3.6. Solution-State NMR Spectroscopy and Computational Studies of **4***

The solution-state behavior of **4** was studied in CD_3OD using variable temperature NMR spectroscopy. The ^{1}H NMR spectrum at ambient temperature contains broad peaks that sharpen upon cooling, suggesting that a dynamic exchange process is responsible for the broadness (Figure 8). Two possible isomers exist for **4** in which the S-atoms remain coordinated**:** the *cis*-isomer observed in the solid state (**4-*cis***) and a *trans*-isomer (**4-*trans***) (Scheme 3). Rapid intramolecular and intermolecular isomerization of group 12 coordination complexes is well documented [29,30], and rapid isomerization between these different isomers at room temperature is a possible

explanation for the dynamic NMR behavior. No efforts to distinguish between intramolecular and intermolecular processes were undertaken.

If **4** retains the **4-*cis*** structure in solution, two sets of proton resonances would be expected for each of the distinct pyridyl ring environments, yielding 11 total resonances for the aromatic region. However, cooling the solution to −38 °C (Figure 8a) produces a ^{1}H NMR spectrum with only 7 resonances in the aromatic region. This is more consistent with a symmetric **4-*trans*** structure having equivalent pyridyl rings, and in fact only 7 resonances are observed throughout the entire temperature range of the experiment, suggesting that no measurable amount of **4-*cis*** is present in solution. Additional low temperature NMR experiments (^{13}C{^{1}H}, HMBC, HSQC and COSY; see supporting information Figures S2–S5) are also consistent with the presence of only a single species having equivalent pyridyl rings.

DFT-optimized structures of the cationic portion of **4-*cis*** and **4-*trans*** were obtained with methanol solvation to gain further insight into the possible solution-phase behavior observed in the NMR experiments (Figure 9). Interestingly, **4-*cis*** is calculated to be ~6 kJ/mol more stable than **4-*trans***, which would lead to **4-*cis*** predominating in solution [31]. However, care should be exercised in interpreting this result since the relative solution-state free energies of these two species could be dramatically affected by interaction with the two weakly-coordinating triflate counterions (which were not explicitly modeled in these calculations), potentially leading to significantly different ratios being observed experimentally.

Of greater usefulness to this analysis are the DFT-predicted NMR spectra of these two species. As was observed for complexes **3a**–**c**, the chemical shift of the C–*H* proton for the bridging methine carbon (H_a) is an important indicator of the binding geometry of the ligand. The calculated ^{1}H NMR spectra of both **4-*cis*** and **4-*trans*** isomers with CH_3OH solvation were compared to the

experimental data for **4** (Table 3), and interestingly H_a is predicted to be the most ***upfield*** of all those in the aromatic region for both isomers (δ = 6.41 and 6.40 ppm, respectively), and not at all consistent with the ~7.5 ppm chemical shift observed for H_a in the low temperature experimental spectrum of **4**. The predicted shifts of **4-*cis*** and **4-*trans*** are similar to the 6.47 ppm value reported for the C–*H* proton in the related tris(2-pyridyl)methane (TPYM) ligand in [Cu(TPYM)CO]ClO_4, where tridentate N,N,N-coordination of the ligand produces no deshielding of the C–*H* proton [32]. Thus, with the presence of no S···H_a interaction in **4-*cis*** and **4-*trans***, the chemical shift would be expected to be similar to that observed for [Cu(TPYM)CO]ClO_4. Instead, the experiments show the chemical shift of H_a in **4** to be more consistent with a solution-state conformation in which it is deshielded by closer proximity to the 2-mercaptoimidazole sulfur.

Taken together, these results suggest that neither **4-*trans*** nor **4-*cis*** predominate in solution, but rather an alternative species is present in which the S-atom is no longer coordinated, yet which still retains equivalent pyridyl groups. Given the long Zn–S bond observed in the crystal structure of **4** and the lack of a Zn–S bond in **3**, dissociation of the 2-mercaptoimidazole sulfur atom is a plausible scenario. Figure 10 shows two such possible alternative structures for the $[(Py_2MeImS)_2Zn]^{2+}$ cation in which the S-atom is not attached and where rotation of the 2-mercaptoimidazole group would place H_a in close proximity to the sulfur (labeled **4′-trans a** and **4′-trans b**). Again, it should be noted that direct coordination of the triflate anions to the zinc center of the $[(Py_2MeImS)_2Zn]^{2+}$ cation would also be likely in such species under experimental conditions, given the roughly square planar ligand environment about the metal and similar coordination of triflate anions in related complexes [33,34]. Nevertheless, the predicted ^{1}H NMR spectra of these cations contain a much more deshielded H_a, which suggest that these or similar species could be present in solution with an uncoordinated S-atom (Table 3) [35]. These results

help to demonstrate the variable coordination geometry possible in solution with the Py_2MeImS ligand and how ^{1}H NMR could yield potential insight into these geometries.

4. Conclusion

A new N_2S ligand bis(pyridyl)(2-mercapto-1-methylimidazolyl)methane (**2**, Py_2MeImS) has been synthesized and characterized. Reaction of the ligand with $ZnBr_2$ resulted in the complex (Py_2MeImS)$ZnBr_2$ (**3**). X-ray analysis of **3** shows bidentate N,N-coordination of the Py_2MeImS ligand resulting in the formation of a boat-like metallocycle, where the uncoordinated 2-mercaptoimidazolyl group is in an equatorial position. The ^{1}H NMR spectrum of **3** at low temperature show two sets of peaks corresponding to two conformers, the likely identity and thermodynamic stability of which were examined using DFT.

Treatment of Py_2MeImS (**2**) with zinc triflate resulted in the homoleptic complex [(Py_2MeImS)$_2$Zn](OTf)$_2$. The solid-state structure revealed an octahedral zinc(II) center coordinated with two Py_2MeImS ligands, where the sulfur atoms are in a *cis*-arrangement. However, variable temperature NMR studies indict a single species in solution that is highly symmetric and inconsistent with the *cis*-isomer observed in the solid-state. DFT calculations proposed alternative structures where the 2-mercaptoimidazole groups are no longer coordinated with the zinc(II) center and the two Py_2MeImS are in a *trans*-arrangement. The computational studies also showed that the chemical shift of the C–*H* proton for the bridging methine carbon ($\boldsymbol{H}_a$) is highly sensitive to whether the sulfur atom of the 2-mercaptoimidazole is in close contact to $\boldsymbol{H}_a$, with the *cis* arrangement resulting in a larger downfield shift for $\boldsymbol{H}_a$. As such, the large downfield shift for $\boldsymbol{H}_a$ in [(Py_2MeImS)$_2$Zn](OTf)$_2$ in the ^{1}H NMR provides evidence that the 2-mercaptoimidazole groups are not coordinated in solution. This is not entirely unexpected based

on the long Zn–S distances observed in the crystal structure. These studies provide valuable insight into the potential binding modes of this new ligand and its behavior in solution.

5. Acknowledgements

This work was supported by an ACS-PRF grant 48483-GB3 to J.T.Y. and a stimulus grant from the Boise State University Graduate College to E.C.B. Summer fellowships to K.E.A. and M.G.C. were provided by an Institutional Development Award (IDeA) from the National Institute of General Medical Sciences of the National Institutes of Health under Grant #P20GM103408 and an NSF-REU Fellowship under Grant #1005159, respectively. The Boise State University NMR facility instrumentation was purchased through an NSF CRIF-MU/RUI (Grant # 0639251) and departmental funding. Mass spectrometry services were provided by the Biomolecular Research Center at Boise State University, which is supported by Institutional Development Awards (IDeA) from the National Institute of General Medical Sciences of the National Institutes of Health under Grants #P20GM103408 and P20GM109095, the National Science Foundation under Grants #0619793 and #0923535, the MJ Murdock Charitable Trust and the Idaho State Board of Education. We gratefully acknowledge Dr. Atta M. Arif at the University of Utah for X-ray structural data collection and refinement.

6. Supporting Information

CCDC 1585875-1585876 contains the supplementary crystallographic data for **3** and **4**. These data can be obtained free of charge via http://www.ccdc.cam.ac.uk/conts/retrieving.html, or from the Cambridge Crystallographic Data Centre, 12 Union Road, Cambridge CB2 1EZ, UK; fax: (+44)

1223-336-033; or e-mail: deposit@ccdc.cam.ac.uk. Low temperature NMR data for **3** (COSY) and **4** ($^{13}C\{^{1}H\}$, HMBC, HSQC and COSY) and atomic coordinates of optimized geometries from DFT calculations are provided.

Table 1. Summary of X-ray crystallographic data and parameters.[a]

Complex	**3**	**4**
Formula	$C_{15}H_{14}Br_2N_4SZn \cdot ½(CH_2Cl_2)$	$C_{32}H_{28}F_6N_8O_6S_4Zn \cdot 1½(CH_2Cl_2)$
Fw	550.02	1055.62
Crystal system	Monoclinic	monoclinic
Space group	$\boldsymbol{P}2_1/n$	$\boldsymbol{P}2_1/n$
a (Å)	12.4751(2)	14.2728(2)
b (Å)	13.1166(3)	12.82460(10)
c (Å)	12.9107(3)	23. 8209(3)
α (deg)	90	90
β (deg)	112.9929(13)	96.2788(6)
γ (deg)	90	90
V (Å^3)	1944.75(7)	4334.09(9)
Z	4	4
D_{calc} (Mg m^{-3})	1.879	1.618
T (K)	150(1)	150(1)
Color	colorless	colorless
Crystal size (mm)	0.20 x 0.15 x 0.13	0.35 x 0.33 x 0.20
Abs coeff (mm^{-1})	5.623	1.023
θ range (deg)	2.47-27.11	2.14-27.47
Completeness to θ (%)	98.5	99.8
Reflections collected	8083	19310
Independent reflections	4222	9905
Parameters	281	557
R1/wR2 (all data)[b]	0.0588/0.1133	0.0605/0.1150
Goodness-of-fit	1.059	1.020
diff. peak/hole (e/Å $^{-3}$)	0.797/-0.901	0.867/-0.814

[a]Radiation used: Mo Kα (λ = 0.71073 Å). [b]R1 = $S||F_o|-|F_c||/S|F_o|$; wR2 = $[S[w(F_o^2-F_c^2)^2]/[S(F_o^2)^2]]^{1/2}$, where $w = 1/[s^2(F_o^2)+(aP)^2+bP]$.

Table 2. B3LYP-calculated ^{1}H NMR chemical shifts for **3a–c** with chloroform solvation (all data in ppm scaled [24] and referenced to TMS; experimental data for Py_2MeImS (**2**) is given in parentheses for comparison; see Chart 3 for H-atom labels).

	2	**3a**	**3b**	**3c**	**Minor**	**Major**
H_a	7.58 (7.64)	8.16	8.17	7.57	8.04	8.23
H_b	7.23 [a] (7.37)	7.13 [a]	8.16	7.12	7.91	8.11
H_c	7.61 [a] (7.72)	7.84 [a]	7.96	7.71	7.91	8.11
H_d	7.19 [a] (7.24)	7.44 [a]	7.56	7.41	7.52	7.75
H_e	8.45 [a] (8.59)	9.00 [a]	8.78	8.84	8.81	8.92
H_f	7.15 (7.27)	6.73	8.17	6.76	8.38	7.83
H_g	6.46 (6.67)	6.82	6.35	6.80	6.91	6.68
H_h	3.31 [a] (3.64)	3.52 [a]	3.32 [a]	3.48 [a]	3.73	3.62

[a]Average calculated values.

Table 3. Experimental ^{1}H NMR chemical shifts for **4** and the B3LYP-calculated data for various isomers of **4** with methanol solvation (all data in ppm scaled [24] and referenced to TMS; see Chart 3 for H-atom labels).

	4	**4-*cis***	**4-*trans***	**4′-*trans* a**	**4′-*trans* b**
H_a	7.48	6.41	6.40	8.48	8.19
H_b	7.44	7.09, 7.77	7.67 [a]	8.25 [a]	7.53
H_c	7.90	7.83, 8.03	7.97 [a]	7.98 [a]	7.91
H_d	7.29	6.84, 7.30	7.41 [a]	7.38 [a]	7.33
H_e	8.55	7.58, 8.93	8.48 [a]	7.82 [a]	7.93
H_f	7.12	7.09	7.17	7.16	7.12
H_g	7.06	6.72	6.72	6.68	7.04
H_h	3.61	3.28 [a]	3.12 [a]	3.45 [a]	3.59 [a]

[a]Average calculated values [35].

Chart 1

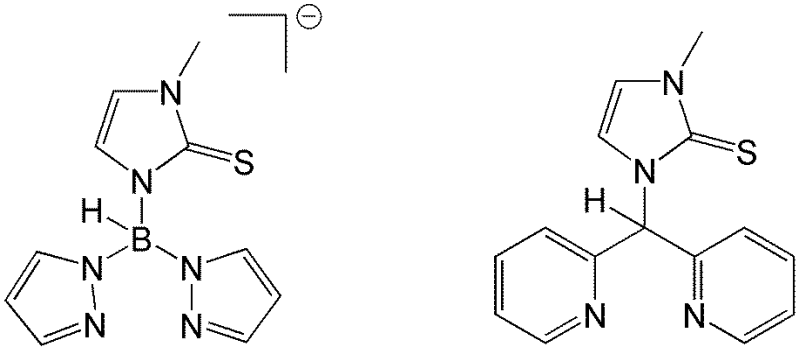

$BpMt^{Me}$ Py_2MeImS

Chart 2

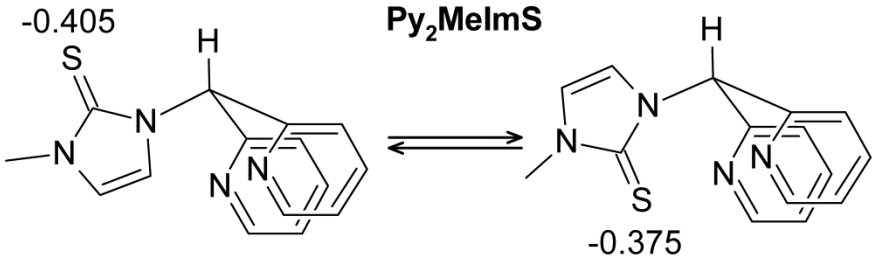

Rotamer a **Rotamer b**

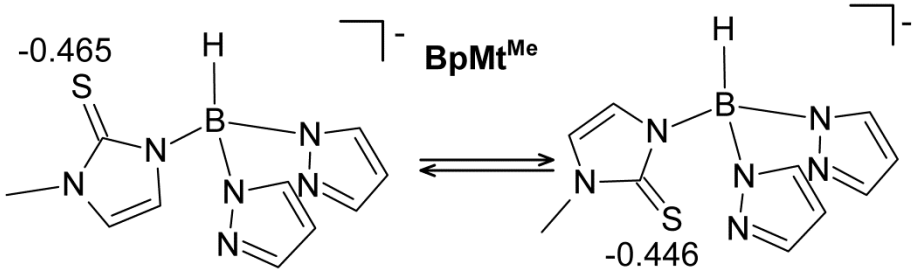

Rotamer a **Rotamer b**

Chart 3.

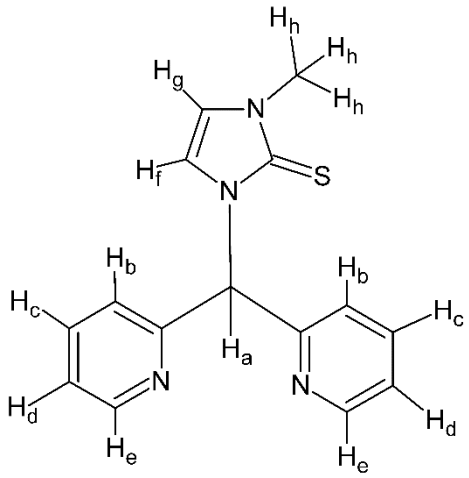

Scheme 1

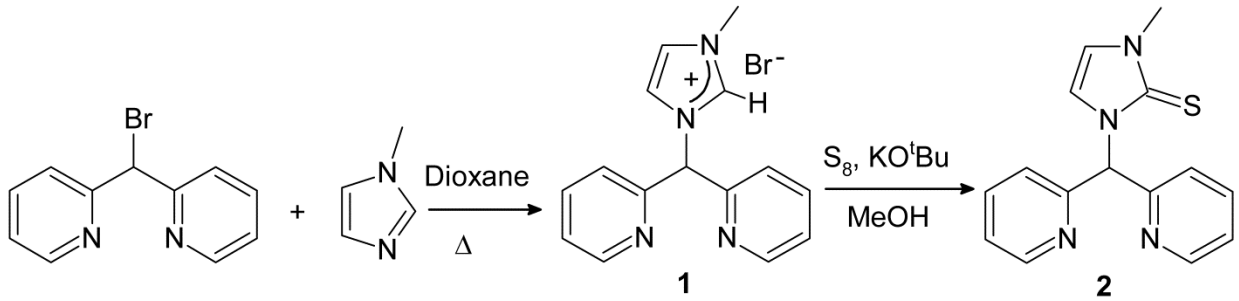

Scheme 2

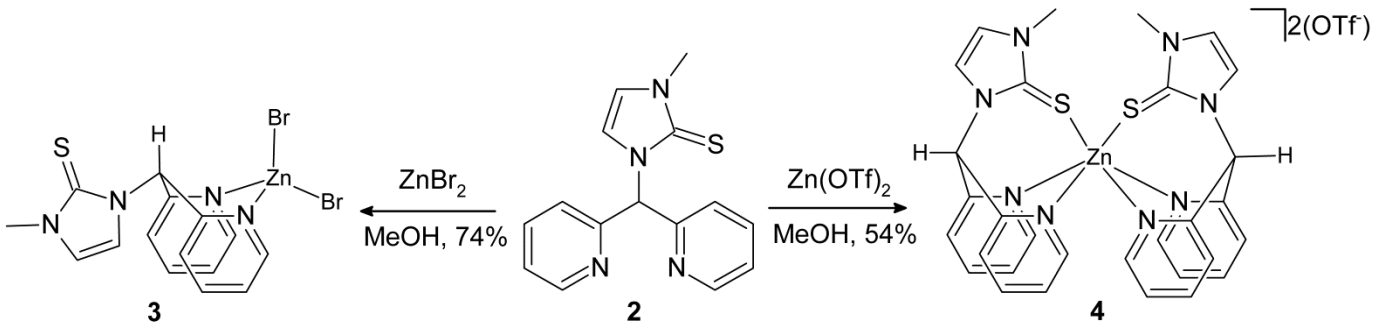

Scheme 3

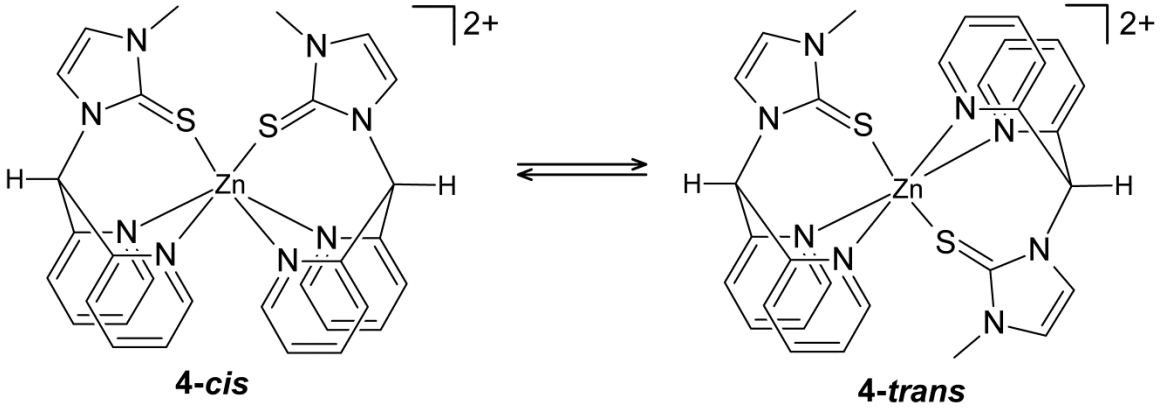

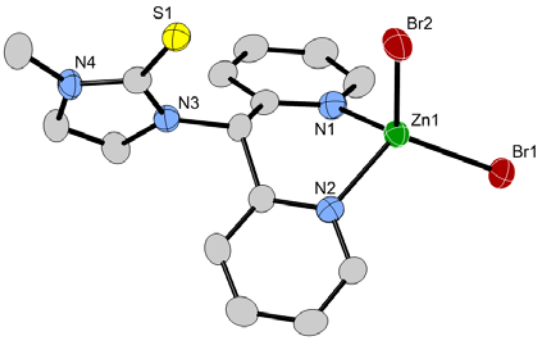

Figure 1. X-ray structure of **3** with thermal ellipsoids drawn at 50% probability level and hydrogen atoms omitted for clarity. Important bond lengths (Å): Zn1–Br1 2.3305(6), Zn1–Br2 2.3515(6), Zn1–N1 2.039(3), Zn1–N2 2.046(3). Bond angles (°): Br1–Zn1–Br2 116.96(2), Br1–Zn1–N1 113.87(9), Br1–Zn1–N2 114.03(9), Br2–Zn1–N1 106.45(9), Br2–Zn1–N2 112.54(9), N1–Zn1–N2 89.56(13).

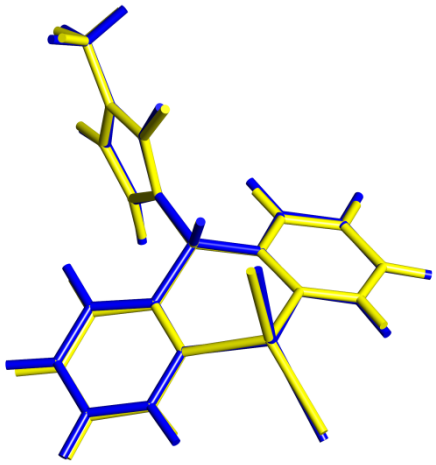

Figure 2. Overlay of the X-ray crystal structure of **3a** (yellow) with the DFT-calculated structure (blue).

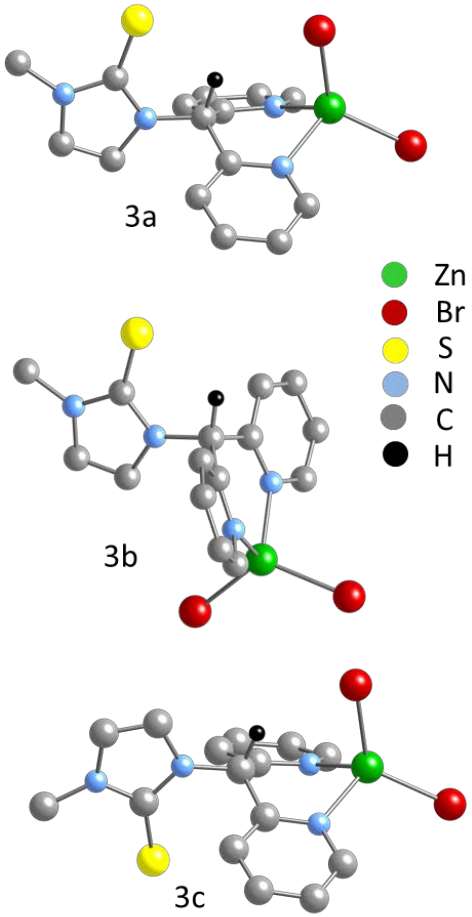

Figure 3. DFT-calculated structures of three possible conformers of (Py_2MeImS)$ZnBr_2$ (**3a–c**) (optimized with $CHCl_3$ solvation; only H_a shown for clarity).

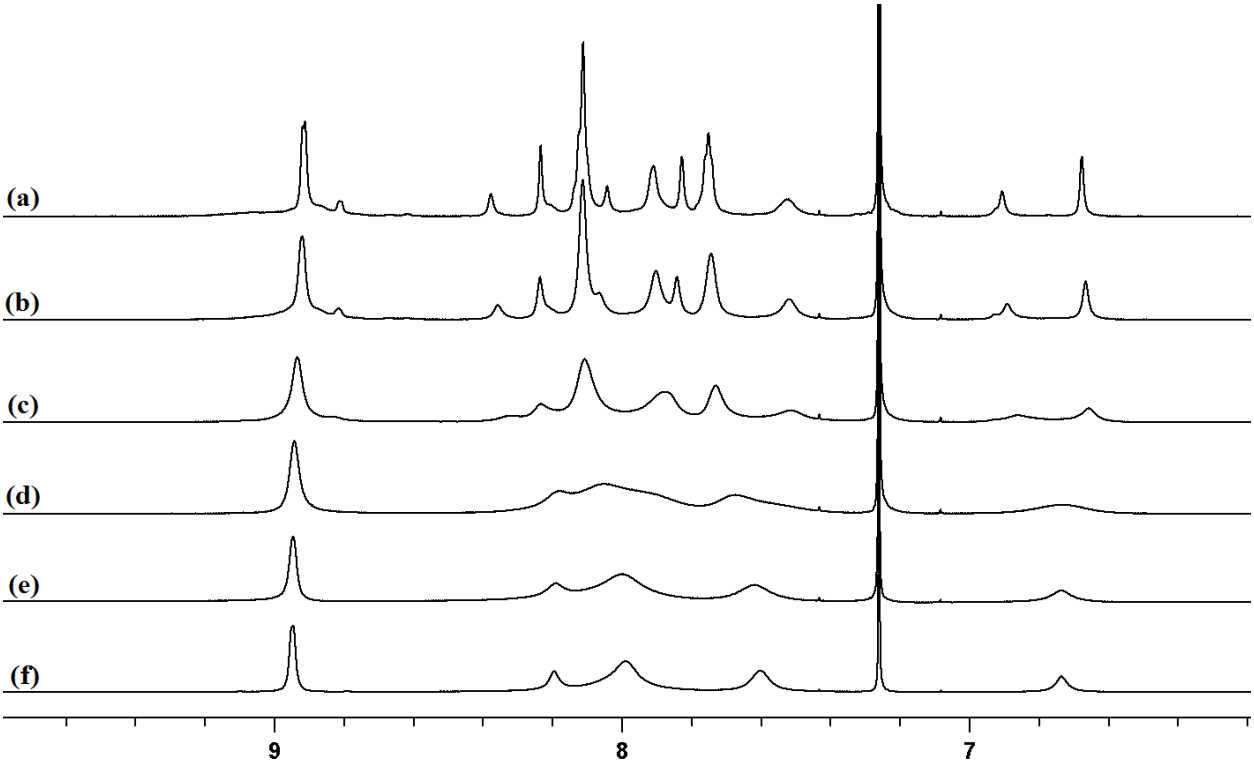

Figure 4. Aromatic region of the ^{1}H NMR spectra of **3** in $CDCl_3$ at a) −48 °C, b) −38 °C, c) −23 °C, d) −3 °C, e) 12 °C and f) 25 °C.

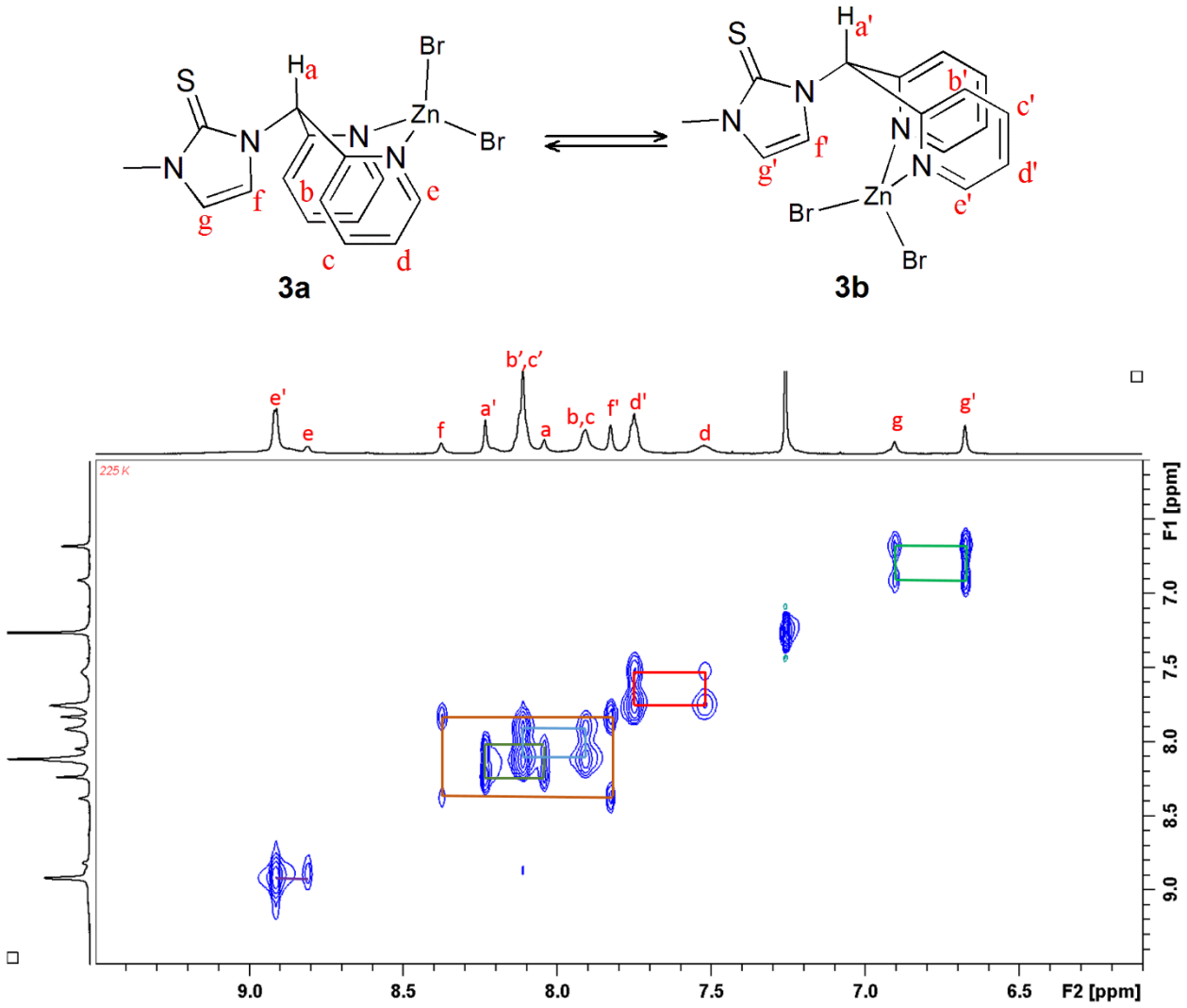

Figure 5. 2D-EXSY spectrum of the aromatic region of **3** in $CDCl_3$ at −48 ºC.

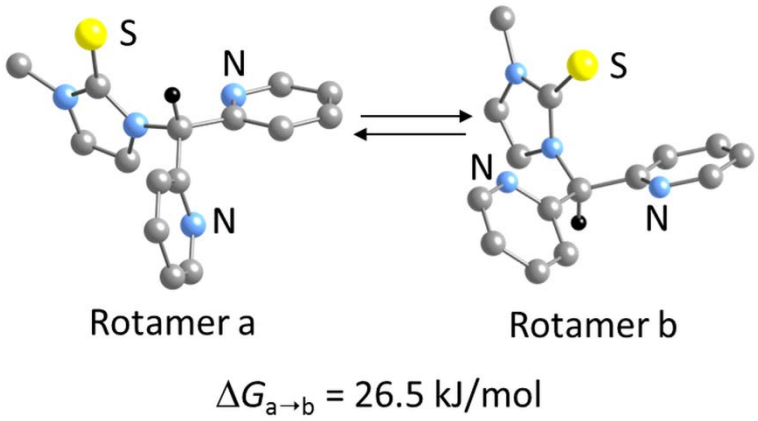

Figure 6. DFT-calculated structures of the two main rotamers of the Py_2MeImS ligand with *H_a cis* to the 2-mercaptoimidazole S-atom (Rotamer a) and with *H_a trans* to the 2-mercaptoimidazole S-atom (Rotamer b) (only *H_a* shown for clarity; relative change in Gibbs free energy shown in kJ/mol with $CHCl_3$ solvation).

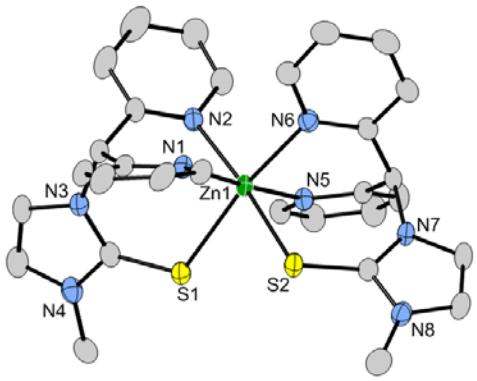

Figure 7. Representation of the cationic portion of the X-ray structure of **4** with thermal ellipsoids drawn at 50% probability level and hydrogen atoms omitted for clarity. Important bond lengths (Å): Zn1–S1 2.5078(7), Zn1–S2 2.5353(7), Zn1–N1 2.210(2), Zn1–N2 2.163(2), Zn1–N5 2.154(2), Zn1–N6 2.161(2). Bond angles (°): S1–Zn1–S2 80.43(2), N1–Zn1–S1 88.57(6), N2–Zn1–S1 96.79(6), N5–Zn1–S1 93.31(6), N6–Zn1–S1 170.75(6), N1–Zn1–S2 89.32(6), N2–Zn1–S2 173.17(6), N5–Zn1–S2 93.33(6), N6–Zn1–S2 90.52(6), N1–Zn1–N2 84.36(8), N1–Zn1–N5 176.97(8), N1–Zn1–N6 93.27(8), N2–Zn1–N5 93.06(8), N2–Zn1–N6 85.26(8), N2-Zn1-N6 85.26(8).

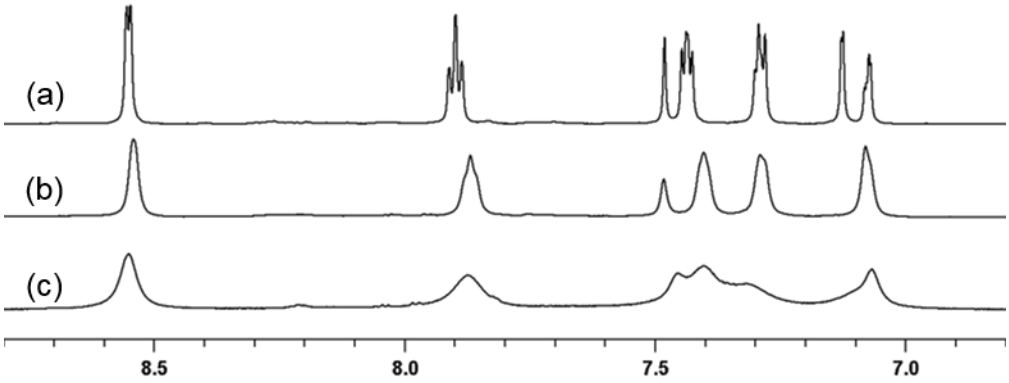

Figure 8. Aromatic region of the ^{1}H NMR spectra of **4** in CD_3OD at a) −38 °C, b) −8 °C and c) 17 °C.

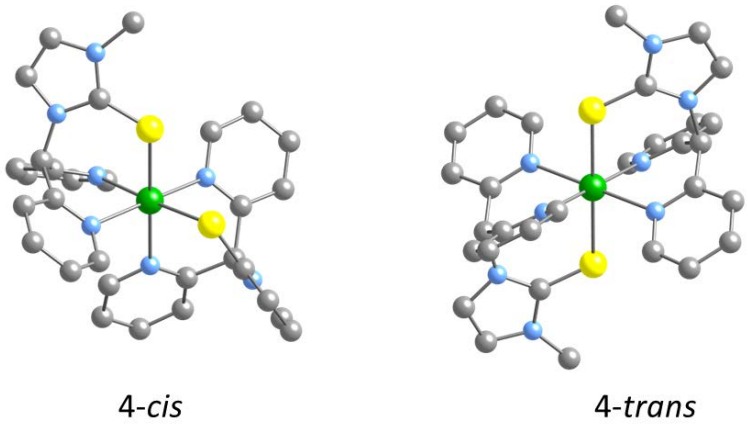

Figure 9. DFT-calculated structures of the *cis* and *trans* isomers of the dication $[(Py_2MeImS)_2Zn]^{2+}$ (**4-*cis*** and **4-*trans***) with coordinated S-atoms (optimized with CH_3OH solvation; H-atoms omitted for clarity).

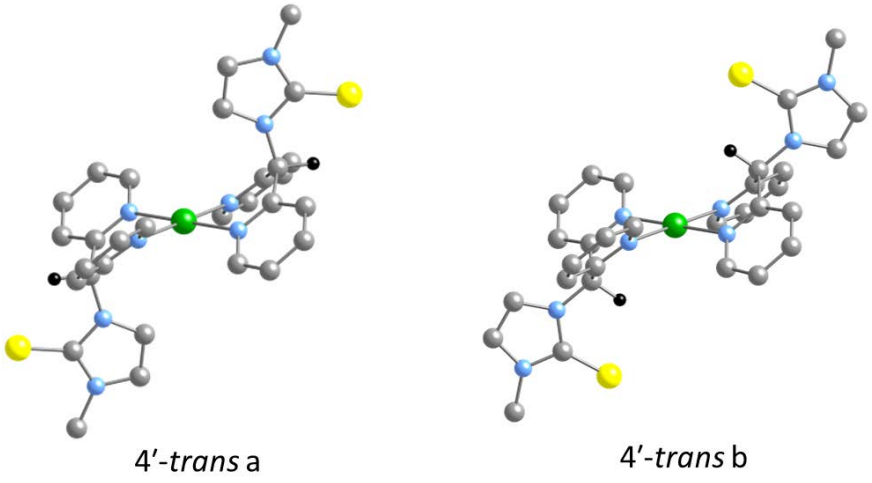

Figure10. Two possible isomers of the dication $[(Py_2MeImS)_2Zn]^{2+}$ (**4**) with uncoordinated S-atoms (optimized with CH_3OH solvation; only H_a shown for clarity).

7. References

[1] (a) M. Inouye, N. Arnheim, R. Sternglanz, R. J. Biol. Chem. 248 (1973) 7247. (b) X. Cheng, X. Zhang, J. W. Pflugrath, F. W. Studier, Proc. Natl. Acad. Sci. 91 (1994) 4034.

[2] A. Serero, C. Giglione, T. Meinnel, J. Mol. Biol. 314 (2001) 695.

[3] A. J. Dent, D. Beyersmann, C. Block, S. S. Hasnain, Biochemistry 29 (1990) 7822.

[4] Representative examples include: (a) P. Ghosh, G. Parkin, Chem. Commun. (1998) 413. (b) B. S. Hammes, C. J. Carrano, Inorg. Chem. 38 (1999) 4593. (c) B. S. Hammes, C. J. Carrano, Inorg. Chim. Acta 300 (2000) 427. (d) B. S. Hammes, C. J. Carrano, Dalton Trans. (2000) 3304. (e) B. S. Hammes, C. J. Carrano, Inorg. Chem. 40 (2001) 919. (f) V. V. Karambelkar, R. C. diTargiani, C. D. Incarvito, L. N. Zakharov, A. L. Rheingold, C. L. Stern, D. P. Goldberg, Polyhedron 23 (2004) 471. (g) E. Galardon, M. Giorgi, I. Artaud, Dalton Trans. (2007) 1047. (h) N. G. Spiropulos, G. C. Chingas, M. Sullivan, J. T. York, E. C. Brown, Inorg. Chim. Acta 376 (2011) 562.

[5] G. Parkin, New J. Chem. 31 (2007) 1996.

[6] F. H. Allen, C. M. Bird, R. S. Rowland, P. R. Raithby, Acta. Crystallogr. B53 (1997) 680.

[7] J. Seebacher, M. Shu, H. Vahrenkamp, Chem. Commun. (2001) 1026.

[8] (a) B. Benkmil, M. Ji, H. Vahrenkamp Inorg. Chem. 43 (2004) 8212. (b) M. Ji, M. Benkmil, H. Vahrenkamp, Inorg. Chem. 44 (2005) 3518. (c) M. Rombach, J. Seebacher, M. Ji, G. Zhang, G. He, M. M. Ibrahim, B. Benkmil, H. Vahrenkamp, Inorg. Chem. 45 (2006) 4571.

[9] A. N. Vedernikov, J. C. Fettinger, F. Mohr, F. J. Am. Chem. Soc. 126 (2004) 11160.

[10] Z. Otwinowski, W. Minor, W. Methods Enzymol. 276 (1997) 307.

[11] A. Altomare, M. C. Burla, M. Camalli, G. L. Cascarano, C. Giacovazzo, A. Guagliardi, A. G. G. Moliterni, G. Polidori, R. J. Spagna, Appl. Cryst. 32 (1999) 115.

[12] G. M. Sheldrick: SHELXL-97. Program for the Refinement of Crystal Structures. University of Göttingen, Germany 1997.

[13] M.J. Frisch, G.W. Trucks, H.B. Schlegel, G.E. Scuseria, M.A. Robb, J.R. Cheeseman, G. Scalmani, V. Barone, B. Mennucci, G.A. Petersson, H. Nakatsuji, M. Caricato, X. Li, H.P. Hratchian, A.F. Izmaylov, J. Bloino, G. Zheng, J.L. Sonnenberg, M. Hada, M. Ehara, K. Toyota, R. Fukuda, J. Hasegawa, M. Ishida, T. Nakajima, Y. Honda, O. Kitao, H. Nakai, T. Vreven, J.A. Montgomery, Jr., J.E. Peralta, F. Ogliaro, M. Bearpark, J.J. Heyd, E. Brothers, K.N. Kudin, V.N. Staroverov, R. Kobayashi, J. Normand, K. Raghavachari, A. Rendell, J.C. Burant, S.S. Iyengar, J. Tomasi, M. Cossi, N. Rega, J.M. Millam, M. Klene, J.E. Knox, J.B. Cross, V. Bakken, C. Adamo, J. Jaramillo, R. Gomperts, R.E. Stratmann, O. Yazyev, A.J. Austin, R. Cammi, C. Pomelli, J.W. Ochterski, R.L. Martin, K. Morokuma, V.G. Zakrzewski, G.A. Voth, P. Salvador, J.J. Dannenberg, S. Dapprich, A.D. Daniels, Ö. Farkas,

J.B. Foresman, J.V. Ortiz, J. Cioslowski, D.J. Fox, GAUSSIAN 09, Revision B.01, GAUSSIAN Inc., Wallingford, CT, 2009.

[14] J.-D. Chai, M. Head-Gordon, Phys. Chem. Chem. Phys., 10 (2008) 6615.

[15] Y. Minenkov, Å. Singstad, G. Occhipinti, V. R. Jensen, Dalton Trans. 41 (2012) 5526.

[16] M. Dolg, U. Wedig, H. Stoll, H. J. Preuss, Chem. Phys. 86 (1987) 866.

[17] (a) M. M. Francl, W. J. Pietro, W. J. Hehre, J. S. Binkley, M. S. Gordon, D. J. DeFrees, J. A. Pople, J. Chem. Phys. 77 (1982) 3654. (b) W. J. Hehre, R. Ditchfield, J. A. Pople, J. Chem. Phys. 56 (1972) 2257.

[18] V. Barone, M. J. Cossi, Phys. Chem. A. 102 (1998) 1995.

[19] R. Krishnan, J. S. Binkley, R. Seeger, J. A. Pople, J. Chem. Phys. 72 (1980) 650.

[20] (a) A. E. Reed, R. B. Weinstock, F. Weinhold, J. Chem. Phys. 83 (1985) 735. (b) A. E. Reed, F. Weinhold, J. Chem. Phys. 83 (1985) 1736.

[21] A. D. Becke, Phys. Rev. A. 38 (1988) 3098. (a) A. D. Becke, J. Chem. Phys. 98 (1993) 5648. (b) C. Lee, W. Yang, R.G. Parr, Phys. Rev. B. 37 (1988) 785. (c) J. P. Perdew, K. Burke, Y. Wang, Phys. Rev. B. 57 (1998) 14999. (d) J. P. Perdew, K. Burke, Y. Wang, Phys. Rev. B. 54 (1996) 16533.

[22] R. Ditchfield, Mol. Phys. 27 (1974) 789. (b) K. Wolinski, J. F. Hilton, P. Pulay, J. Am. Chem. Soc., 112 (1990) 8251. (c) J. R. Cheeseman, G. W. Trucks, T. A. Keith, M. J. Frisch, J. Chem. Phys., 104 (1996) 5497.

[23] G. K. Pierens, T. K. Venkatachalam, D. C. Reutens, Scientific Reports 7 (2017) 5605.

[24] G. K. Pierens J. Comp. Chem. 35 (2014).

[25] (a) R. Alsfasser, H. Vahrenkamp, Inorg. Chim. Acta 209 (1993) 19. (c) N. Galván-Tejada, S. Bernès, S. E.Castillo-Blum, H. Nöth, R. Vicente, N. Barba-Behrens, J. Inorg. Biochem. 91 (2002) 339.

[26] A. Nimmermark, L. Öhrström, J. Reedijk, Zeitschrift für Kristallographie - Crystalline Materials 228 (2013) 311.

[27] K. A. Haushalter, J. Lau, J. D. Roberts, J. Am. Chem. Soc. 118 (1996) 8891.

[28] (a) H. M. Alvarez, T. B. Tran, M. A. Richter, D. M. Alyounes, D. Rabinovich, J. M. Tanski, Inorg. Chem. 42 (2003) 2149. (b) J. Nunn, I. Zahedi, G. Bauer, M. F. Haddow, S. N. Abdul Halim, A. Pérez-Redondo, G. R. Owen, Inorg. Chim. Acta 365 (2011) 462. (c) J. R.

Miecznikowski, W. Lo, M. A. Lynn, B. E. O'Loughlin, A. P. DiMarzio, A. M. Martinez, L. Lampe, K. M. Foley, L. C. Keilich, G. P. Lisi, D. J. Kwiecien, C. M. Pires, W. J. Kelly, N. F. Kloczko, K. N. Morio, Inorg. Chim. Acta 376 (2011) 515.

[29] (a) S. M. Berry, D. C. Bebout, R. J. Butcher, Inorg. Chem. 44 (2005) 27. (b) W. Lai, S. M. Berry, D. C. Bebout, Inorg. Chem. 45 (2006) 571. (c) D. C. Bebout, W. Lai, S. M. Stamps, S. M.; Berry, R. J. Butcher, Polyhedron 27 (2008) 1591.

[30] (a) W. Yang, H. Schmider, Q. Wu, Y. Zhang, S. Wang, Inorg. Chem. 39 (2000) 2397. (b) A. Beitat, S. P. Foxon, C. Brombach, H. Hausmann, F. W. Heinemann, F. Hampel, U. Monkowius, C. Hirtenlehner, G. Knör, S. Schindler, Dalton Trans. 40 (2011) 5090.

[31] While the highest symmetry point group possible for **4-*trans*** is C_{2h}, optimization with this symmetry constraint yielded a structure with a small imaginary frequency (-4.7 cm^{-1}). Subsequent optimization with C_i symmetry yielded a minimum-energy structure with no imaginary frequencies and a lower energy than the C_{2h}-symmetric structure (by 5.1 kJ/mol). A C_2-symmetric minimum-energy structure was also found, but it is higher in energy than the C_i-symmetric structure by 3.6 kJ/mol. The relative energy of **4-*cis*** and **4-*trans*** isomers was therefore determined from the energy of the **4-*trans*** isomer having C_i symmetry. The ^{1}H NMR chemical shifts reported in Table 3 for **4-*trans*** are for the C_i-symmetric structure, with average values given for inequivalent protons. Notably, these average values are very similar to the values obtained for the C_{2h}-symmetric structure, indicating that the exact point group symmetry does not significantly affect the calculated chemical shifts in this complex.

[32] M. Kujimi, T. Kurahashi, M. Tomura, H. Fujii, Inorg. Chem. 46 (2007) 541.

[33] (a) J. Börner, U. Flörke, A. Döring, D. Kuckling, M. D. Jones, S. Herres-Pawlis, Sustainability 1 (2009) 1226. (b) W. Yang, H. Schmider, Q. Wu, Y.-S. Zhang, S. Wang, Inorg Chem. 39 (2009) 2397.

[34] For the dication $[(Py_2MeImS)_2Zn]^{2+}$, the calculated energies of the **4′-*trans a*** and **4′-*trans b*** conformers in solution are significantly higher than the most stable **4-*cis*** structure [(by 78.8 and 46.0 kJ/mol, respectively). However, likely coordination of the two triflate anions directly to the zinc(II) center in **4′-*trans a*** and **4′-*trans b*** in solution to yield a six-coordinate metal center could dramatically affect the energies of these and similar compounds relative to the six-coordinate **4-*cis*** and **4-*trans*** species in which the triflate anions are not coordinated to the metal center. Thus, the relative energies of the different conformers of $[(Py_2MeImS)_2Zn]^{2+}$calculated without explicit treatment of the triflate anions is not necessarily indicative of their relative energies under experimental conditions.

[35] As with **4-*trans***, both **4′-*trans a*** and **4′-*trans b*** can ideally possess C_{2h} symmetry. However, optimization of **4′-*trans a*** with C_{2h} symmetry yielded a single small imaginary frequency (-24.0 cm^{-1}). Optimization of **4′-*trans a*** with C_i symmetry yielded a minimum energy structure with no imaginary frequencies, and the reported ^{1}H NMR chemical shifts for this complex are listed. However, because all pyridyl protons are not exactly equivalent in this structure, average values of these are reported. These average values are similar to the values

obtained for the C_{2h} structure, indicating that the exact point group symmetry does not significantly affect the calculated chemical shifts in this complex.